9.1.6 Battery Selection

It should be noted that NiCd batteries can only be used where there is a simple requirement for steady runtime voltage and reliability. NiCd cells are not as low-cost as their lead-acid counterparts, but the low capacity density prevents their use in the majority of applications. In PV systems, the battery implementation can be either for stationary energy storage or in mobile applications. Lead-acid, NiMH, lithium-ion, and NaS batteries are all widely available for such uses. The following tips can be considered for selecting among them.

- *Lithium-ion technology* is suitable for different scales and applications, has high performance in terms of capacity density, and is becoming cheaper due to recent mass production. Detailed sensing and protection should always be used to guarantee safe operation, especially for systems with significant storage capacity.
- *Lead-acid batteries* can be selected for either vehicular or stationary implementations. Their advantages lie in the maturity of the technology and their low cost. The drawbacks are the low capacity density per unit weight and volume.
- *NaS technology* has potential for large-scale stationary energy storage due to its high operating temperature. However, the supply is limited to a single source, which is different from the other technologies.
- *NiMH batteries* can be used for small-scale PV systems for either vehicular or stationary implementations when the power density is not critical. The technology is generally low cost, but has shorter life cycles, higher self-discharge rates, a memory effect, and is inefficient in comparison with lithium-ion batteries.

9.2 Integrating Battery-charge Control with MPPT

Charging is the process of storing solar power in discharged batteries. A suitable charging method should be used to charge them efficiently and prevent any damage. To stop the PV generation from overloading the charging capacity, the charging cycle should be maintained with an MPPT function.

When the voltage and current of the battery reach their charging-cycle limits, MPPT should be stopped in order to reduce PV power generation. Instead, the control action should shift the operating point of the PV generator in the open-circuit voltage direction or into the voltage-source zone. It has been reported that the system dynamics of the voltage-source zone gives better damping performance than the current-source zone (Xiao et al. 2007). The PV I–V curve has been divided into three operating zones: current-source zone, power-source zone, and voltage-source zone, as shown in Figure 6.2. It is recommended to operate the PV output in the power-source and voltage-source zones and to avoid the current-source zone.

Figure 9.28 illustrates the integration of MPPT and cycle-charge control, in terms of constant voltage and constant current regulation. For battery-charging applications, the battery voltage and current are sensed to determine the operation status. If both are under their defined limits, MPPT is used to deliver the highest charging power. If either limit is reached, the control variable moves the operating point away from the MPP, in the direction of the open-circuit voltage. For the case study, ±1% hysteresis is applied to the regulation for both battery voltage and battery current. The hysteresis error can

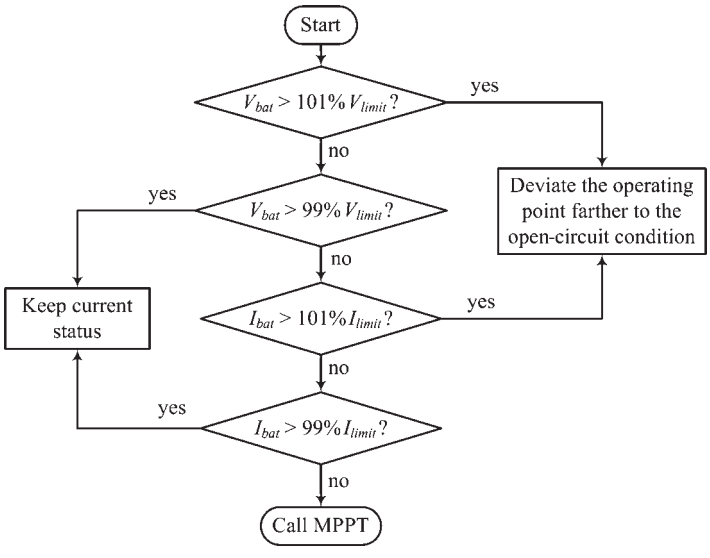

Figure 9.28 Integration of maximum power point tracking for battery charge control.

be other values depending on the practical requirements. When the sensed voltage and current are within their predefined tolerances, the controller maintains the steady-state condition.

9.3 Design of Standalone PV Systems

This section introduces the design, integration, and simulation of standalone PV power systems. The systems may or may not include significant energy storage. "Significant" energy storage means that the storage capacity is sufficient to mitigate the intermittency of PV generation. Switching-mode power supplies contain energy storage units, such as inductors and capacitors, to constrain switching noise, which is considered insignificant in comparison with batteries.

9.3.1 Systems without Significant Energy Storage

Most DC loads can be supplied with a certain range of DC voltage. A direct-coupled system is the simplest solution and can be designed to match the PV module with the load demand. An example is used to demonstrate the design procedure. A solar-powered ventilation system is required to provide airflow up to 700 CFM (cubic feet per minute). A cooling fan is selected to meet the airflow requirement, the specifications for which are shown in Table 9.9. A PV module should be selected to match the supply voltage range and the power requirement.

To match the voltage range from 18 to 30 V, as shown in Table 9.9, a PV module is constructed from 48 crystalline solar cells. The size of the solar cells is 6 inches, with a current rating of 7.20 A. A suitable PV module is selected, and the specification is shown in Table 9.10. The rated MPP of the PV module is close to the rated voltage and current required by the cooling fan. The peak power at STC is 170 W, which is slightly lower than

Table 9.9 Specification of Orion 12HBXC01A cooling fan.

Term	Rating
Model number	NMB F225A4-092-D0530
Nominal voltage	24 V
Nominal current	7.20 A
Voltage range	18–30 V
Rated power	172.8 W
Rated air flow	763 CFM

Table 9.10 Specification of Invensun i170-48P PV module.

Basic information					
Manufacturer	Model	Cell material	Dimension		
Invensun	i170-48P	Poly-crystalline	1316 mm × 995 mm × 40 mm		
Electrical performance at STC					
Cells	P_{MPP}	I_{MS}	V_{MS}	I_{SCS}	V_{OCS}
48	170 W	7.14 A	23.81 V	7.72 A	28.8 V
Temperature coefficients					
	α_T	β_T	γ_T		
	0.06%/°C	−0.35%/°C	−0.45%/°C		

α_T, β_T, and γ_T are temperature coefficients for correcting the PV module output current, voltage, and power, respectively.

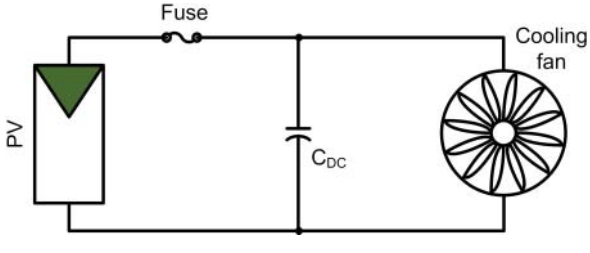

Figure 9.29 System diagram of direct coupled PV system for ventilation.

the rated power of the load, 172.8 W. The system can safely operate at 170 W, without being overloaded.

The system is shown in Figure 9.29. A DC-link capacitor gives a start-up current and maintains a steady voltage at the DC link. The fuse is rated as 15 A, in line with the recommendation in the PV module datasheet.

Although direct coupling is the simplest solution, it is very difficult to achieve an exact match between the off-the-shelf load and the PV generator when variation of environmental conditions is a factor. In many cases, the system design is customized for either the load or the PV unit. Simulation for case studies can be conducted only if the I–V

characteristics of the PV module and the load are available. However, the manufacturer of the cooling fan does not provide such information. Experimental testing therefore becomes important.

It should be noted that many cooling fans monitor the input voltage and apply autostart and stop based on the voltage level. If such a function is not supported or does not fit the PV output curve, an additional control circuit should be included to support the start and stop function with a hysteresis loop. In this case, the voltage window of the load is 18–30 V. The voltage threshold for start can be set to 24 V or higher to ensure that the PV module can support enough power at the start point. Without the hysteresis setting, the system can start and stop frequently in the early morning since the irradiance level is not sufficient to support the nominal operating power even though the open-circuit voltage is high enough.

Without power-conditioning circuits, the MPPT function cannot be implemented. This hints that the PV module mostly operates away from the peak power point due to the variation of environmental conditions. Therefore, more and more recent PV systems are including power-conditioning units, to allow use of MPPT and flexibility in design and operation. A direct-coupled system can be redesigned to integrate a dedicated power conditioner.

One important application is proposed by Mascara NT, a French company, which supplies highly efficient off-grid systems for seawater desalination. The concept is simple, since fresh water is only produced when solar power is available. The system stops at night or when the weather is bad. The "storage" is fresh water instead of any electrical format. Even though no significant battery storage is required, power conditioning is included in the conversion stage between the PV section and the load. Reverse osmosis is used for high-efficiency desalination. Solar power drives the pump motor and supplies ancillary devices. A DC bus is formed from multiple PV strings in order to directly supply the desalination unit.

9.3.2 Systems with Significant Energy Storage

When energy storage is required, system design generally follows six steps, as shown in Figure 9.30 and described in the following steps:

1) The load profile should be clearly specified, including the daily energy consumption and the rated voltage. The energy consumption is measured in Wh or kWh for a 24-h period. The nominal load voltage is the reference for rating the battery pack and solar generation unit voltages.

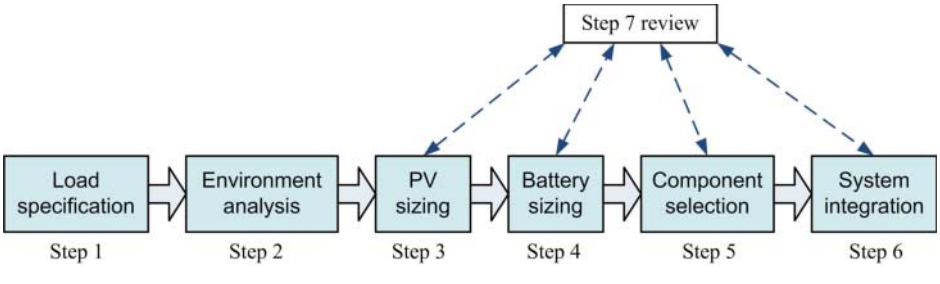

Figure 9.30 A design procedure for PV-battery systems.

2) The location should be thoroughly examined to derive information about the level of solar irradiance and ambient temperatures. It is known that solar irradiance is directly correlated with PV power generation. High temperatures can degrade power generation. It should be noted that the analysis is based on rough estimates since the exact weather cannot be accurately predicted.
3) The rule for sizing the PV generation unit is based on the daily load consumption and the lowest solar generation period. PV generation should be more than the load consumption over a 24-h period. The PV generation unit can be slightly oversized to deal with uncertainty.
4) The voltage of the battery pack should be specified to match the load voltage rating in order to avoid a high ratio of voltage conversion. The battery capacity should be sufficient to mitigate the power variation between daytime generation and nighttime load consumption. The possibility of a deep charge/discharge cycle – more than 60% – should be minimized since it accelerates battery aging. The capacity of the battery pack should generally be oversized by 20–30% to cope with charge and discharge losses.
5) The system should be designed according to the specifications of the load, PV generation unit, and battery pack. DC/DC and/or DC/AC converters might be used according to the load requirement. Protection and disconnect functions should be included. A complete schematic should be presented for review.
6) The design document should include a single line diagram of the system structure, showing all component ratings and details.
7) The final step is to review the whole system specification and design. The design can be revised if any outstanding issues are raised.

The design process can be demonstrated by an example. The load specification is shown in Table 9.11. The 24-h energy consumption, E_{load}, is calculated to be 3200 Wh using (9.6). According to the voltage rating, a battery pack rated at 48 V should be used to meet the acceptable voltage-variation range.

$$E_{load} = 140 \times 8 + 130 \times 16 \tag{9.6}$$

Step 2 is to evaluate the environmental conditions at the installation location. The information collected is shown in Table 9.12. It should be noted that it is impossible to predict any weather condition accurately. Extreme weather is not included in this design process due to its unpredictability. Since the highest temperature is not significantly higher than STC, the power degradation caused by high temperatures can be neglected in this example.

Table 9.11 Specification of DC load.

Term	Rating
Nominal voltage rating	48 V DC
Acceptable voltage range	42–56 V
Averaged power consumption from 9am to 5pm	140 W
Averaged power consumption at other hours	130 W

Table 9.12 Weather information for PV power generation.

Term	Rating
Average irradiance in 8 h period year round	600 W/m^2
Low irradiance in 8 h period on rainy days	200 W/m^2
Average high temperature over year	25.9°C
Average low temperature over year	8.1°C

Step 3 is to size the PV power generator unit. The solar power generation is expected to be sufficient even though the average irradiance is only 200 W/m^2 on rainy or cloudy days. The daily energy generation should be more than 3200 Wh, which is the daily load requirement. The rated power of the PV unit should be calculated from the 8-h generation limit in a 24-h base period, corrected for any estimated losses. The minimum PV power capacity is calculated to be 2500 W, with a 20% loss expected in the power conversion:

$$P_{STC} = \underbrace{\frac{1000}{200}}_{\text{irradiance}} \times \underbrace{3200}_{\text{load}} \times \underbrace{\frac{1}{1-20\%}}_{\text{loss}} \times \underbrace{\frac{1}{8}}_{\text{8-hour}} \tag{9.7}$$

Step 4 is to size the battery pack to store excess energy produced by the PV unit and supply the load at night. It is estimated that there will be 16 h without any solar energy input in a 24-h period. According to the load profile, the minimum energy capacity of the battery is 480 Wh, with a cycle between 0% and 100%. It is commonly recommended to operate the battery in a light cycle, from 40 to 90%, for long operational life. Therefore, the nominal energy capacity of the battery pack is rated as 4160 Wh:

$$E_{bat} = \underbrace{\frac{1}{90\% - 40\%}}_{\text{battery cycle}} \times 16 \times 130 \tag{9.8}$$

Based on the requirements for its capacity, the battery capacity in C rate terms can be rated as 87 Ah from

$$C_{bat} = E_{bat}/V_{b-nom} \tag{9.9}$$

where V_{b-nom} refers to the nominal voltage of 48 V in this case. The battery pack can be formed from four 12-V battery modules in series connection. The BK-10V10T battery modules are used to form the battery pack, since each is rated at 12 V and 90 Ah.

A solar charge controller is used to maintain the battery charging cycle and maximize PV generator output. The FLEXmax 60 used is manufactured by Outback Power Inc. The key specifications are shown in Table 9.13. Further information can be found on the product website at www.outbackpower.com.

The voltage rating of the PV string should match the input voltage window of the charge controller, which should not be higher than 150 V in cold conditions. The voltage at MPP should be higher than the open-circuit voltage of the battery pack at 100% SOC. In this case, the voltage window is from 56 to 150 V in order to construct the PV string.

Table 9.13 Key specification of the charge controller–FLEXmax 60.

Term	Rating
Nominal battery voltage	Programmable for 12, 24, 36, 48, or 60 V
Maximum output current	60 A
Maximum input voltage	150 V
Voltage conversion	Step down

Table 9.14 Specification of PV module Q.PLUS BFR-G4.1.

Basic information					
Manufacturer	Model	Cell material	Dimensions		
Q Cells	Q.Plus BFR-G4.1	Multi-crystalline	1000 mm × 1670 mm × 32 mm		
Electrical performance at STC					
Cells	P_{MPP}	I_{MS}	V_{MS}	I_{SCS}	V_{OCS}
60	280 W	8.84 A	31.67 V	9.41 A	38.97 V
Temperature coefficients					
	α_T	β_T	γ_T		
	0.04%/°C	−-0.29%/°C	−0.40%/°C		

α_T, β_T, and γ_T are the temperature coefficients for correcting the PV module output current, voltage, and power, respectively.

The Q.Plus BFR-G4.1 solar module is selected for this application. It is produced by Hanwha Q Cells GmbH. The key specifications at STC are shown in Table 9.14. Detailed and updated information is found at the product website at www.q-cells.com.

Nine PV modules are required for this application, since each is rated at 280 W. The total power capacity is 2520 W, which is higher than the fundamental requirement of 2500 W at STC. The modules can be configured into three strings, each with a number of PV modules in series (N_{series}) of 3. The maximum DC voltage is calculated as the sum of the rated open-circuit voltage of each string, with correction for the lowest expected temperature:

$$V_{pvdc}(\max) = K_T \times 3 \times 38.97 = 116.91K_T \tag{9.10}$$

where K_T is the correction factor. The installation location is expected to become as cold as 8.1°C, and K_T can be as determined from the temperature coefficients listed in Table 9.14. Using (9.11) it can be calculated as 1.17. Therefore, the maximum DC voltage is rated as 137 V, lower than the 150 V required by the charge controller. At the STC, the string voltage at MPP is 95 V. Even though the MPP voltage is lower when the temperature is higher than 25°C, the voltage rating at MPP should be always higher than the minimum requirement of 56 V in order for the step-down voltage conversion that is required by the battery-charge controller.

$$K_T = 1 + \beta_T(8.1 - 25) \tag{9.11}$$

Figure 9.31 is the single line diagram for the standalone system configuration. The specifications of the charge controller and PV module are shown in Tables 9.13 and 9.14. The information about other key components, the battery pack, PV source circuit, DC combiner, DC disconnect, and DC circuit breakers, are summarized in Tables 9.15–9.19 and 9.20, respectively. Together with the climate information for the installation site, the diagram and tables should be included in the final design document. It should be noted that the 48-V battery system requires a higher voltage rating for the circuit components interconnected with the battery voltage bus because of the expected battery voltage variation.

Even though AC loads are common in many standalone systems, these can be equivalent to DC loads since a DC/AC power interface is required to draw DC power from the system. DC/AC conversion systems have been discussed in various books on the subject of power electronics. Therefore the subject is not covered in this book. For a

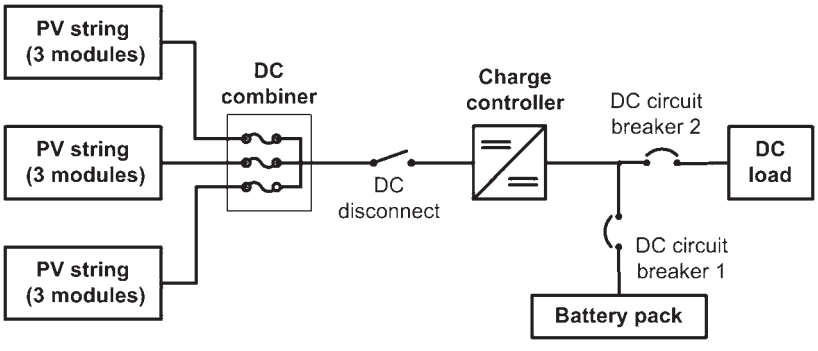

Figure 9.31 Single line diagram of standalone PV system with battery storage.

Table 9.15 Battery pack configuration and specification.

Term	Rating or description
Configuration	4 battery modules in series connection
Battery pack voltage rating	48 V
Battery pack nominal capacity	90 Ah
Battery module model	Panasonic BK-10V10T
Battery type	Nickel metal hydride (NiMH)

Table 9.16 Configuration and specification of PV source circuit.

Term	Rating or description
PV array configuration	3 PV strings in parallel connection
PV string configuration	3 PV modules in series connection
Maximum array voltage rating	137 V
Maximum array current rating	35.3 A

Table 9.17 Configuration and specification of DC combiner.

Term	Rating or description
Configuration	No less than three inputs
Rating of string protection fuse	15 A
Voltage rating	Not less than 137 V

Table 9.18 Specification of DC disconnect.

Term	Rating or description
DC disconnect current rating	Not less than 44 A
DC disconnect voltage rating	Not less than 137 V

Table 9.19 Specification of DC circuit breaker 1.

Term	Rating or description
Amperage rating	90 A
Voltage rating	Not less than 56 V
Configuration	With integrated DC disconnect

PV–battery system, it is always good practice to minimize the use of AC loads due to the loss and complications of DC/AC conversion. More and more modern equipment and appliances are using DC supply.

9.4 Equivalent Circuit for Simulation and Case Study

The equivalent circuit for simulation can be derived from the system design in Figure 9.31. Figure 9.32 illustrates the equivalent circuit for analysis and simulation. The simplified Thévenin model is used, and includes the battery pack voltage V_{OC} and the equivalent series resistance R_{bat}. The dynamics of the battery link shows interaction with the capacitor, C_{BAT}, which is the equivalent capacitance across the battery pack. All DC loads are simplified to draw current from the battery link, which is denoted as i_{load}. A buck converter is the charge controller that transfers the PV power to the battery and supplies the load. The inductor current of the buck converter is denoted i_L. The circuit dynamics are

$$i_L + i_{bat} = C_{BAT}\frac{dv_{bat}}{dt} + i_{load} \tag{9.12}$$

and

$$R_{bat}C_{BAT}\frac{di_{bat}}{dt} + i_{bat} = i_{load} - i_L \tag{9.13}$$

with the assumption of a constant voltage, V_{OC}, in the short-term steady state.

Table 9.20 Specification of DC circuit breaker 2.

Term	Rating or description
Amperage rating	5 A
Voltage rating	Not less than 56 V
Configuration	With integrated DC disconnect

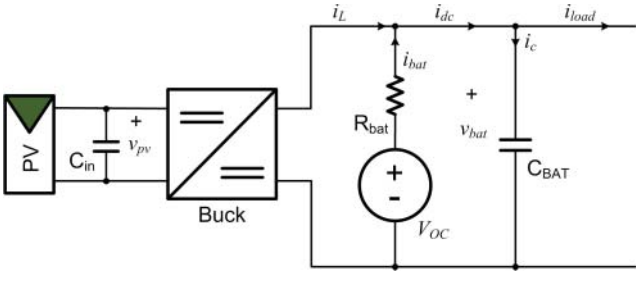

Figure 9.32 Equivalent circuit of standalone PV system with battery storage.

The battery-link dynamics can also be represented by the transfer function:

$$i_{bat}(s) = \frac{i_{load} - i_L}{R_{bat}C_{BAT}s + 1} \tag{9.14}$$

In the steady state, the battery current, i_{bat}, is the error between the load current i_{load} and the inductor current of the buck converter i_L. The aggregated capacitance across the battery terminals causes the dynamics at the battery link.

9.5 Simulation Model to Integrate Battery-charging with MPPT

MPPT using the HC algorithm was introduced in Section 8.2 and formulated for simulation, as illustrated in Figure 8.6. With the integration of battery-charging cycles, a control flowchart for the PV-powered battery charger can be developed, as shown in Figure 9.28. The Simulink model should integrate the MPPT and the regulation of the battery voltage and current.

Figure 9.33 illustrates the simulation block in Simulink. The bottom section shows the HC operation for tracking the MPP. The MPPT operation can update the control variable only if both the battery voltage and current are within their limits, which are indicated by 0.99Vlimit and 0.99Ilimit. The system is operated in MPPT mode.

If either the battery voltage or current reaches its predefined limit, the system enters the charging-cycle mode. Either the battery voltage or current is regulated to avoid battery overcharging. When the value of either the battery voltage or current is within a 2% tolerance range, the model output Xnew is maintained constant by setting the variation step to zero. However, if either the battery voltage or current reaches their upper limits, denoted 1.01Vlimit and 1.01Ilimit, respectively, the control action will move the

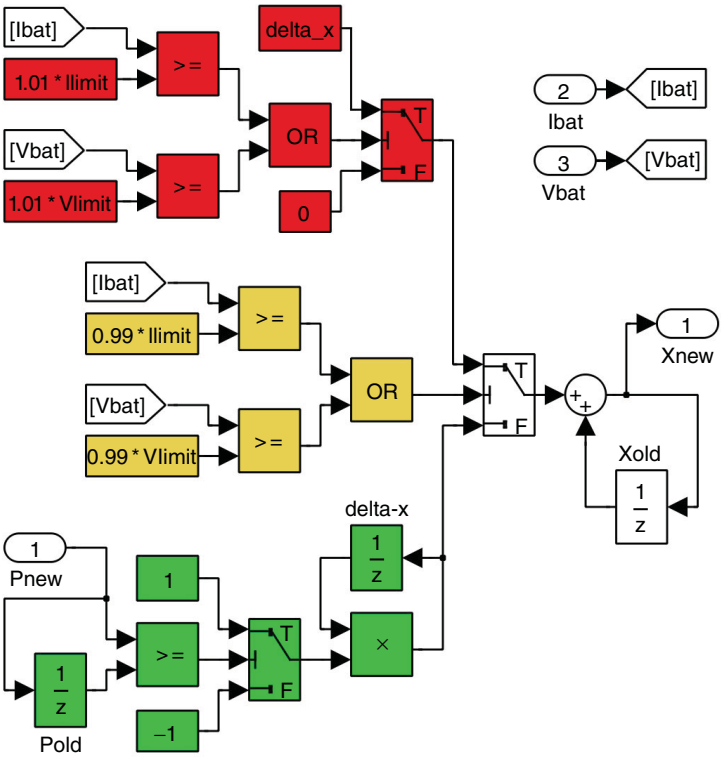

Figure 9.33 Simulink model for integrating MPPT and battery-charging cycles.

operating point in the direction of the open-circuit voltage by updating the value of Xnew. In this case, Xnew is the PV output voltage. Therefore, increasing its value brings it closer to the open-circuit condition. It should be noted that the 2% tolerance, from 99% to 101%, is just as an example for this case study. Other values can be assigned to maintain the battery voltage and current within a limited range.

9.6 Simulation Study of Standalone Systems

A simulation model for the designed system is needed to assess its response to changes of environmental conditions and load variations. The simulation system is based on the case study and design in Section 9.3.2.

9.6.1 Simulation of PV Array

The PV cell parameters can be estimated using the specification of the PV module shown in Table 9.14. The PV cell voltage is derived from the module output voltage and the number of cells in series connection. Based on the ideal single-diode model (ISDM), the ideality factor of the PV cell is determined as 1.6882.

The PV array that was developed in Section 9.3.2 has a 3×3 configuration of nine PV modules. Therefore, the PV array output characteristics at STC are represented by the

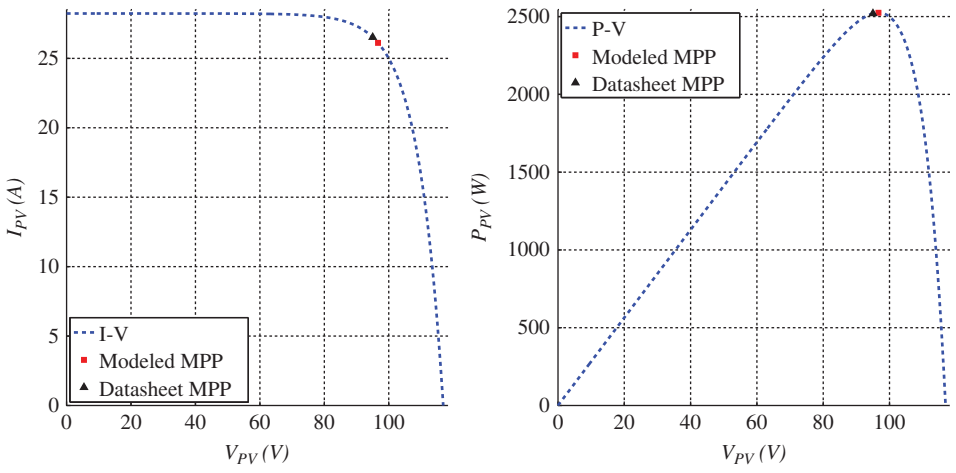

Figure 9.34 Output characteristics of the 3 × 3 PV array.

I–V and P–V curves shown in Figure 9.34. With balanced operation of nine PV modules, the MPP of the array is indicated as 2525 W and is at (96.66 V, 26.12 A).

9.6.2 Short-term Simulation

Figure 9.35 shows the overall model for simulating the standalone system including the PV array, DC/DC buck converter, battery link, and battery pack. The blocks for the solar irradiance, cell temperature, and the load current represent subsystems to be programmed to vary as predefined conditions. It should be noted that the sign of the battery current is defined as positive when it is extracted from the battery pack. Modeling of the buck converter used as the PV-side converter was introduced and developed in Section 5.1.2. The model is capable of capturing the dynamics during each switching cycle. For the case study, the specification of the buck converter is as shown in Table 9.21. The same parameters are used for the medium-term and long-term simulations described in later subsections.

The system control is represented by the blocks for the MPPT charger, PID controller, and PWM generator. The PID controller and PWM generator are those developed in Section 7.8.3. Based on the nominal operating condition and circuit parameters, as shown in Table 9.21, a small-signal model can be derived using the modeling process in Section 6.3.2. The model has a damping factor of 0.26 and an undamped natural frequency of 1.08×10^3 rad/s. Affine parameterization is used to design the feedback controller to regulate the PV-side voltage in order to follow the MPP. As a result, the PID controller for the voltage regulation of the PV link is synthesized and expressed as

$$C(s) = -0.0017 - \frac{8.4736}{s} - \frac{6.8485 \times 10^{-6}}{2.8745 \times 10^{-4} s + 1} \tag{9.15}$$

The MPPT charging block is implemented as shown in Figure 9.33. The MPPT parameters are summarized in Table 9.22. The tracking frequency should always be determined by the dynamic analysis of the PV-link voltage-regulation loop. Without the start-stop mechanism, as introduced in Section 8.6, a 1-V ripple is expected to

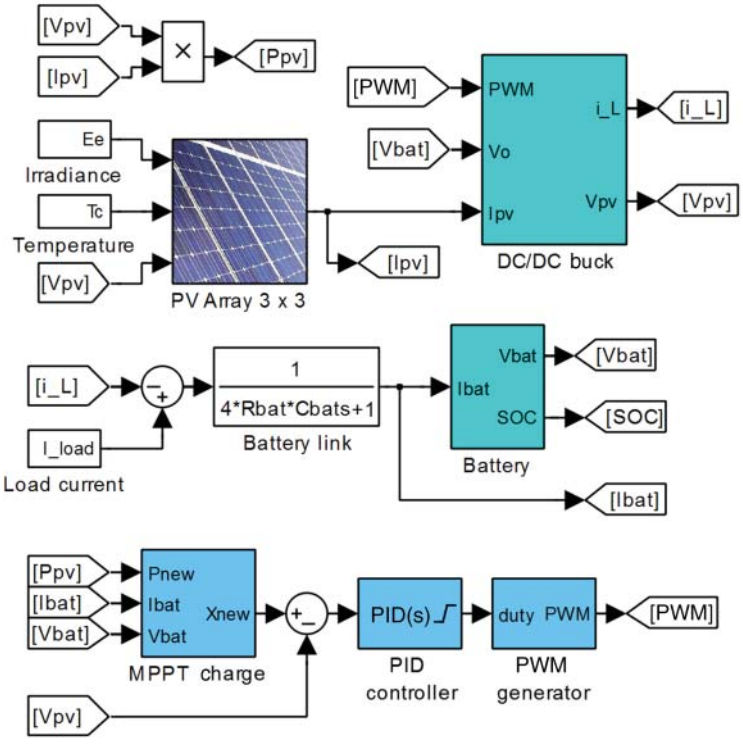

Figure 9.35 Configuration of the standalone PV system with battery storage for short-term simulation.

Table 9.21 Specification of buck converter circuit.

Term	Rating or description
Switching frequency	50 kHz
Inductance	L = 470 μH
Input capacitor	C_{in} = 470 μF
Nominal input voltage	95 V
Nominal output voltage	48 V

Table 9.22 Specification of the MPPT algorithm.

Term	Rating or description
MPPT algorithm	Hill-climbing method
MPPT tracking frequency	200 Hz
Perturbation step size	ΔV = 1 V

appear in the PV-link voltage due to the active perturbation of the HC algorithm. The equivalent capacitance across the battery link is set to $C_{bat} = 33$ μF for the case study.

To avoid battery overcharging, the upper limit of the battery voltage is set to 55 V, which represents the series connection of 40 NiMH cells in the case study. Since a 2% (±1%) tolerance is applied, the band for the voltage limit is between 54.45 and 55.55 V. When the battery voltage is higher than 54.45 V, active tracking of the MPP is stopped and charge control is taken to maintain the battery voltage within the upper limit of the tolerated range.

The simulation model of the buck converter, as shown in Figure 5.6, is computationally intensive due to the fast switching frequency of 50 kHz. The sampling time for simulation should be at a level of nanoseconds to capture the switching dynamics and reveal the detailed transient responses up to the switching frequency. The model is suitable for the total simulation times in seconds in order to prove the design concept of the converter circuit and monitor switching ripples, since the battery voltage is relatively steady over short time periods. The detailed simulation model is inefficient for either medium- or long-term simulations for demonstration of the variation of battery SOC and voltage during charging and discharging. Therefore, the simulation results are neglected for this case study since they have been covered in Section 5.1.2.

9.6.3 Medium-term Simulation

The averaged model was introduced in Section 6.3.2. It is based on the assumption that the buck converter is in continuous conduction mode. The expression in (6.17) can be further derived as

$$i_L = \frac{1}{L}\int (d v_{pv} - v_{bat})dt \tag{9.16a}$$

$$v_{pv} = \frac{1}{C_{in}}\int (i_{pv} - d i_L)dt \tag{9.16b}$$

where d is the switching duty cycle and the control variable. Other variables and parameters refer to the definitions in Figure 9.32.

Figure 9.36 illustrates the simulation blocks for the averaged model of the DC/DC buck converter. The inputs include the duty cycle, the output voltage, and the PV injection current, which are labeled duty, Vo, and Ipv, respectively. The output variables are the inductor current and the PV terminal voltage. The control variable for the averaged converter model is the value of the duty cycle instead of the PWM pulsed signals.

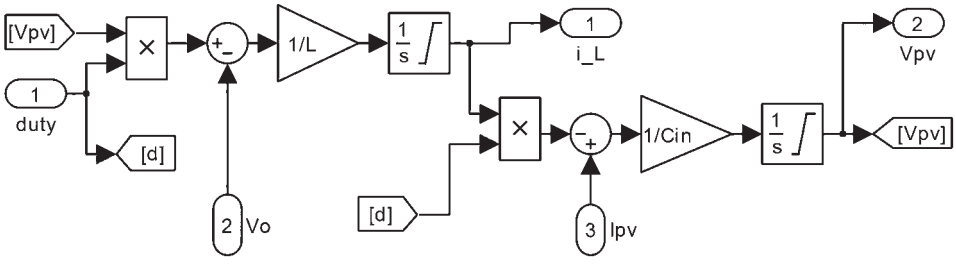

Figure 9.36 Simulink model of the averaged synthesis of the buck converter.

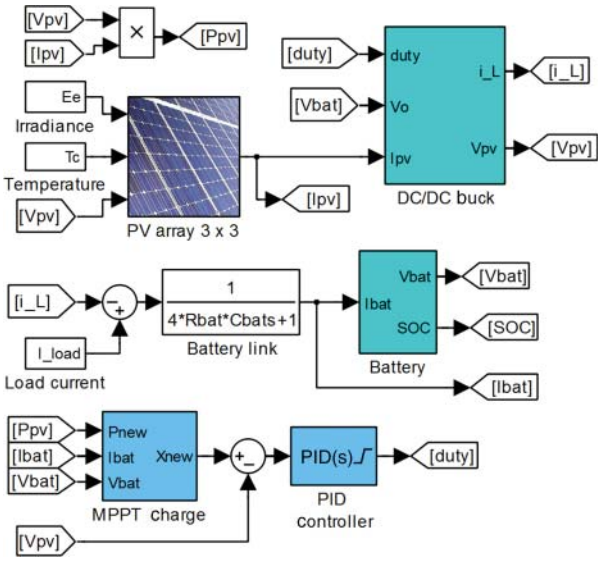

Figure 9.37 Configuration of standalone PV system with battery storage for medium-term simulations.

The switching ripples will not be expected in the simulated waveform of the PV-link voltage and the inductor current.

Figure 9.37 illustrates the block diagram when the averaged model is used to represent the DC/DC buck converter. The key difference from the switching model in Figure 9.35 is that the input of the DC/DC buck converter model is the value of the duty cycle. The high-frequency PWM signal and switching operation are neglected in the averaged model to improve simulation speeds. The control parameters are kept the same as shown in Tables 9.22 and (9.15). The battery link is represented by the transfer function (9.14). The battery model was as developed in Section 9.1.5 and shown in Figure 9.18.

The simulation result of the case study is illustrated in Figure 9.38. The initial SOC of the battery pack was set to be 50%. A load current of 2.8 A was constantly extracted from the battery link. Before 0.2 s, the irradiance was 400 W/m^2 and the cell temperature was 25°C. Since the battery voltage is lower than the limit of 54.45 V, the MPP is tracked at 0.09 s during the start-up period and maintained by the steady-state tracking operation. The voltage ripple caused by the active perturbation of the HC algorithm is noticeable. The SOC gradually increases in response to the charging current. At 0.2 s, the solar irradiance steps up from 400 to 800 W/m^2. The PV output power significantly increases, causing an increase of the charging current. The increase of the SOC becomes faster than before. Since the SOC is still relatively low, the battery voltage is still below the upper limit. The MPPT operates continuously so as to inject the highest power into the battery link.

Figure 9.39 illustrates the simulated waveform for another case study. The initial SOC of the battery pack is set to be 80%. Again, a constant load current of 2.8 A is extracted from the battery link. Before 0.2 s, the irradiance is 400 W/m^2 and the cell temperature is 25°C. Since the battery voltage is lower than the limit of 54.45 V, the MPP is tracked at 0.09 s and is maintained by the steady-state tracking operation for the highest solar

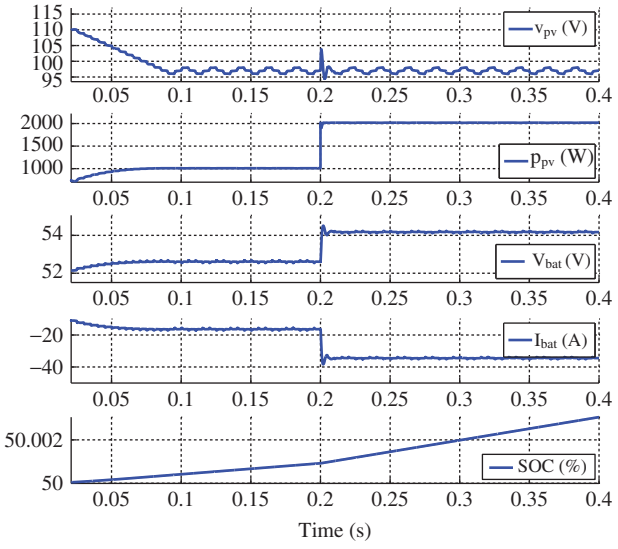

Figure 9.38 Simulated waveforms showing maximum power point tracking for battery charging.

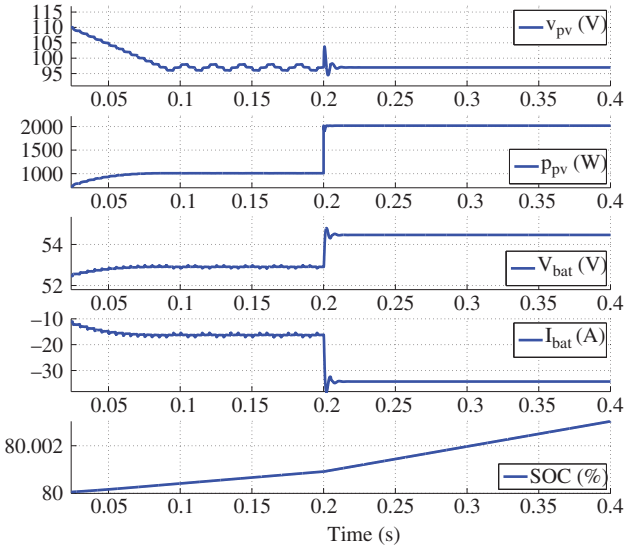

Figure 9.39 Simulated waveforms showing the transition from maximum power point tracking to battery voltage regulation.

energy harvest. The SOC gradually increases in response the charging current. At 0.2 s, the solar irradiance steps up from 400 to 800 W/m^2. The PV output power is significantly increased, causing the increase of the charging current, which is represented as negative in value. Since the SOC is at a relatively high level, the battery voltage reaches the predefined limit due to the equivalent resistance of the battery pack. The active tracking for MPP is stopped, as can be seen from the disappearance of the tracking ripple.

The charging control maintains the battery voltage within the upper limit range. The charging continues, and the SOC increases within the simulation time period of 0.4 s.

Figure 9.40 shows the simulated waveform for the third case study. The initial SOC is 80%, and the load current is a constant 2.8 A. Before 0.2 s, the irradiance is 800 W/m^2 and the cell temperature is 25°C. Since the battery voltage reaches the limit of 54.45 V, the system uses battery voltage regulation to maintain the charging cycle. The PV output voltage is maintained at a level higher than the voltage of the MPP in order to maintain low output power. At 0.2 s, the solar irradiance steps down from 800 to 400 W/m^2. The PV output power significantly decreases, causing a decrease of the charging current. Since the battery voltage becomes lower than the limit of 54.45 V, active MPPT is started. It is noticeable that the MPPT operation lowers the PV output voltage to a lower level for the highest power output under an irradiance level of 400 W/m^2. The ripple appears again on the waveform of the PV-link voltage. This is caused by the perturbation operation of the HC-based MPPT.

A sudden load change can cause a disturbance to the battery current. It might trigger a transition between MPPT and battery voltage regulation. The variation can also represent a change of the PV output power. Therefore, a case study for load variation is not presented in this section.

The voltage-regulation loop of the buck converter exhibits the highest frequency at the kilohertz level. This requires the simulation sampling time to be at the microsecond level in order to capture the fastest dynamics. For this reason, the averaged model is not efficient for simulation of long-term operations, where there are significant changes of battery SOC and voltage in response to changes in environmental conditions and load. Simulations might result in significant demands for memory and computing speed, which is impractical on standard personal computers.

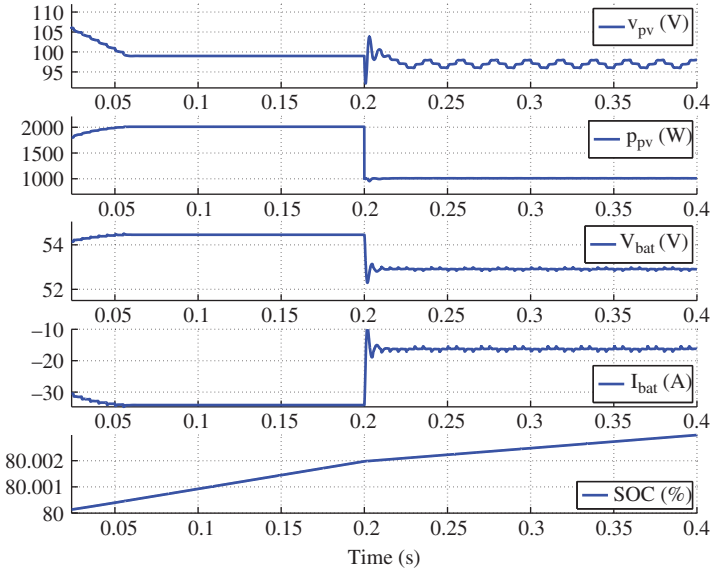

Figure 9.40 Simulated waveforms showing the transition from the battery voltage regulation to maximum power point tracking.

9.6.4 Long-term Simulations

The computer configuration for the simulation cases in this book is shown in Table 9.23. This is considered as a suitable platform to test the simulation efficiency.

It commonly takes hours to charge a battery from low capacity to full. For a long-term simulation, the fast dynamics of the buck converter and the battery link can be neglected. The equilibrium of the buck converter from input to output in continuous conduction mode without the consideration of losses can be expressed as

$$i_L = \frac{i_{pv}}{d} \tag{9.17a}$$

$$d = \frac{V_{bat}}{v_{pv}} \tag{9.17b}$$

where d is the switching duty cycle and the control variable. Other variables and parameters refer to the definitions in Figure 9.32. The dynamics caused by the capacitor, inductor, and switching operation are ignored.

The model of the standalone PV system with battery storage for long-term simulation can be constructed as shown in Figure 9.41. The model simply shows an energy correlation between the PV array and the battery pack. The buck converter is represented by (9.17). The voltage of the PV link is the direct output of the MPPT charge controller with the assumption that the PV array voltage follows the command much faster than the MPPT dynamics. The control functions for MPPT and the regulation of the battery voltage and current are the same as for the short- and medium-term simulations. The highest frequency in the simulation model becomes the MPPT frequency, which is 200 Hz. Therefore, the sampling frequency for simulation can be set to 2 kHz in order to simulate the system efficiently.

Figure 9.42 shows the simulated waveform for a two-hour system operation. The initial SOC of the battery pack is set to be 50%. Again, the load current is 2.8 A, constantly extracted from the battery link. For 40 min, the irradiance is 400 W/m^2 and the cell temperature is 25°C. Since the battery voltage is lower than the limit of 54.45 V, the MPP is tracked and maintained for the highest solar energy harvest. A voltage ripple appears in the waveform of the PV-link voltage, v_{pv} due to the perturbation of the HC algorithm. The SOC gradually increases in response the charging current.

After 40 min, the solar irradiance changes from 400 to 800 W/m^2. The PV output power significantly increases, causing an increase of the charging current. Since the SOC is at a medium level, the battery voltage is still below the voltage limit. Therefore, MPPT operates for 38 min and gives a fast increase of the SOC. After 68 min, active MPPT is stopped because the battery voltage rises to a level of of 54.45 V. The system

Table 9.23 Specification of the simulation computer.

Term	Specifications
Computer model	Dell Precision T1650
Operating system	Windows 10 Pro, 64-bit
Processor	Single Intel® i7-3770 core, 3.4 GHz
Installed memory (RAM)	16 GB

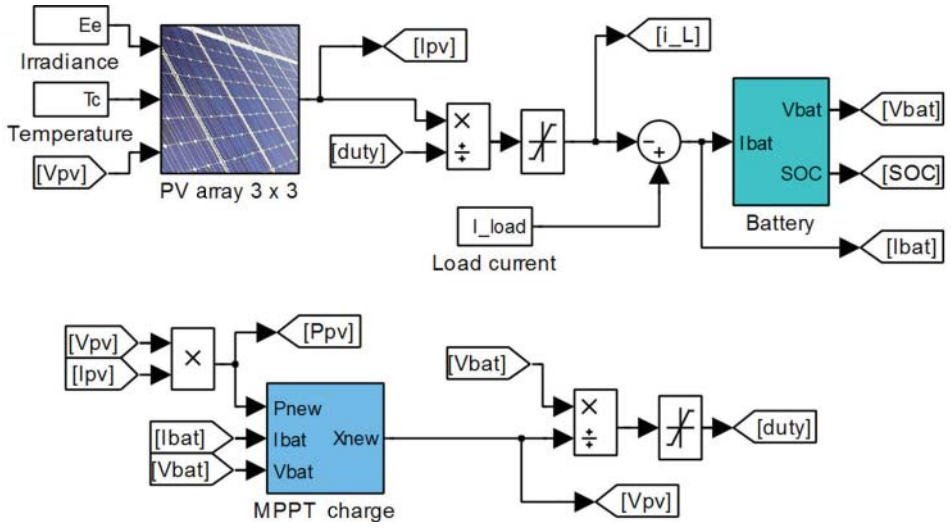

Figure 9.41 Configuration of standalone PV system with battery storage for long-term simulation.

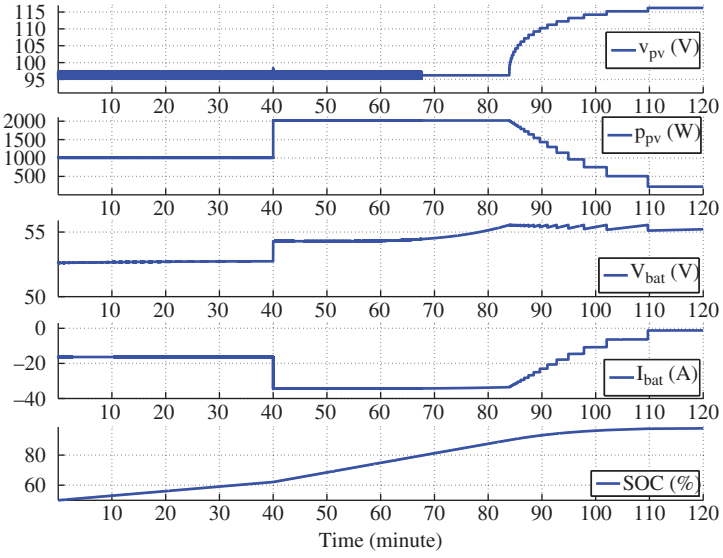

Figure 9.42 Simulated waveforms showing the two-hour operation.

is maintained at the same charge condition until the battery voltage reaches the upper level of 55.55 V. After 84 min, the charge controller takes action to increase the PV-link voltage from the MPP. The deviation of the MPP lowers the PV output power and the charge current, even though the PV array is potentially capable of reaching the higher power level. The battery voltage is regulated for continuous charging until the battery is fully charged, which can be sensed by a reduction of the battery charging current. PV generation is maintained to supply the load power consumption. Using the simplified model, the total simulation time is 7 min for two hours of system operation showing

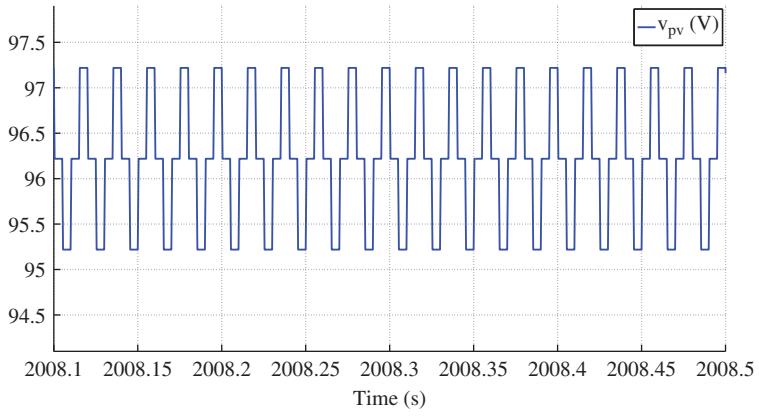

Figure 9.43 Simulated waveform of the PV-link voltage, illustrating the details of MPPT.

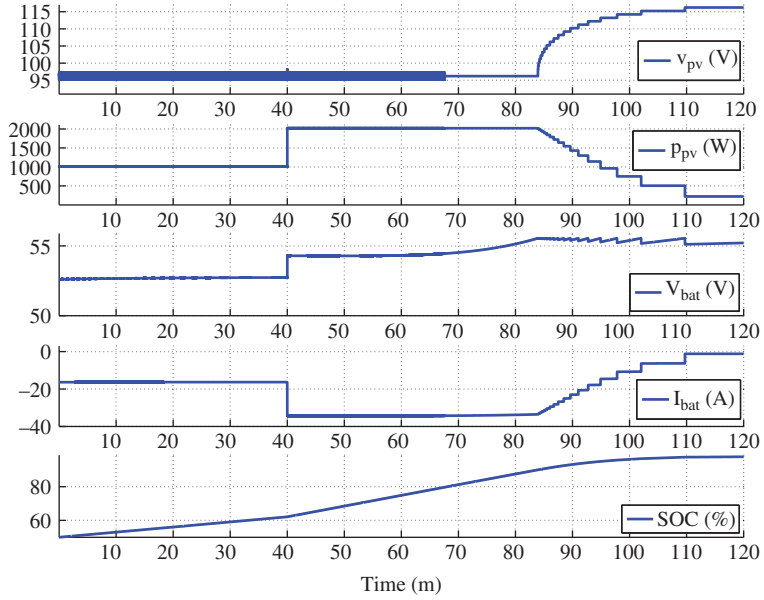

Figure 9.44 Simulated waveforms for the two-hour operation.

the detailed operation of the MPPT algorithm and charging cycle regulation. Figure 9.43 shows a zoom-in on the waveform of the PV-link voltage, v_{pv}. It reveals the perturbation details around the MPP in the early stages due to the operation of the HC algorithm.

In the simulation model, as shown in Figure 9.41, the highest frequency is represented by the HC algorithm, which is in discrete-time format. In contrast to simulations to capture continuous signals, this allows the sampling frequency to be set at up to twice the frequency, which is 400 Hz. For the same two-hour period of operation discussed above, the simulation time is reduced to 63 s, rather than the 7 min in the previous study. The simulation result is shown in Figure 9.44, which is visually identical to the waveform in Figure 9.42, which reflects the cycle charge and MPPT operation.

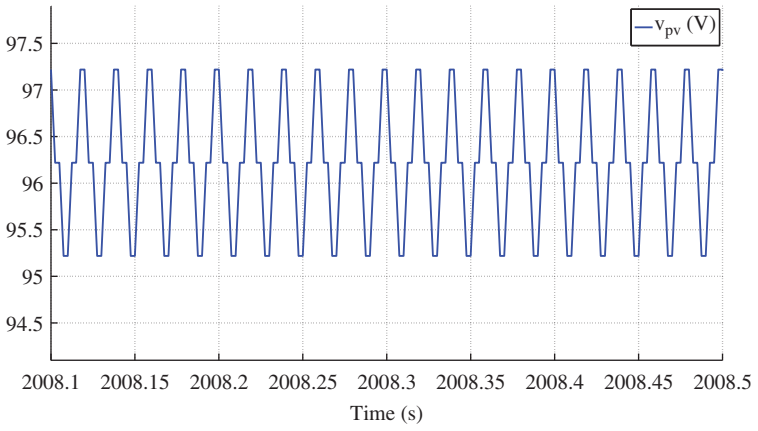

Figure 9.45 Simulated waveform of the PV-link voltage illustrating the MPPT detail.

Figure 9.45 is a zoom-in on the waveform of the PV-link voltage, v_{pv}. It clearly shows the perturbation around the MPP due to the operation of the HC algorithm, but the details are not as accurate as the waveform in Figure 9.43. If the waveform details are not critical, the reduced sampling frequency can significantly improve the simulation efficiency for long-term simulation studies.

9.6.5 Very-long-term Simulations

The proposed method is capable of simulating even longer-term operations with the simplified model and a reduced sampling frequency. When environmental data, such as irradiance and temperature, are available, the simulation can be used to predict the PV power system output in voltage and current terms. Using the same environmental data as the study by Xiao et al. (2013), the long-term simulation can be extended to eight-hour operation.

Figure 9.46 shows the simulated waveforms for the irradiance, cell temperature, PV-link voltage, battery voltage, PV output power, battery current, and battery SOC. It took 7.5 min to simulate the eight hours of system operation. The simulation result can be explained as follows:

- The irradiance increases from the early morning to its highest point in the middle of the day and decreases in the afternoon. The temperature also changes to its highest point at the middle of the day and decreases to lower level in the evening. The temperature variation affects the PV-link voltage representing the MPP, which is high at low temperatures and low at high temperatures. The solar irradiance significantly affects the PV output power.
- The initial SOC of the battery pack after the overnight discharge is 30%. The battery voltage is relatively low at the start point.
- MPPT operates at the beginning of the system control operation so as to inject the highest available power into the battery link. Ripples appear in the waveform of the PV-link voltage, indicating the active perturbation from the HC-based MPPT algorithm. The simulation shows that the system tracks the MPP at each moment and regulates the PV string voltage to follow the MPP.

- The control mode is switched to battery voltage regulation after the first 3.1 h of operation, until the battery voltage reaches the first upper limit of 54.45 V. The PV output and charge current continuously increase to respond to variations in solar irradiance.
- The system is maintained in the steady state for 15 min while the battery voltage is between 54.45 V and 55.55 V. The MPP of the PV array is no longer tracked during this period.
- Battery voltage regulation starts when the battery voltage reaches the upper limit of 55.55 V. The PV-link voltage is controlled to rise and deviate from the MPP. The PV output power and charge current are reduced by the deviation of the MPP, even though the PV array has the potential for higher power output.
- The regulation of the battery voltage is maintained for another 3 h until the solar irradiance drops to a low level in the late afternoon. The PV array output is regulated to maintain the load requirement and the float charge of the battery pack. The SOC is maintained at 100%.
- In the last hour of operation, the irradiance is close to zero. The battery is switched from charge to discharge mode. The load current is at the predefined value of 2.8 A. The battery voltage and SOC decrease accordingly. The operating mode will last until the next morning when solar radiation becomes available.

The simulation of the eight hours of operation shows the major drawback of standalone systems. The system is significantly oversized to accommodate bad weather conditions and low irradiation. However, solar energy is simply wasted on sunny days, as shown in this case study. The simulation result shows that the system takes the full power generation from the PV array for the first three hours. Then the control action curbs the PV power output in order to maintain constant voltage for the battery pack. Therefore, grid-connected systems represent a great advantage since the electrical network can usually absorb the PV power without limiting the generation.

9.7 Summary

Energy storage has high potential to mitigate the intermittent power generation of renewable resources. Several battery technologies were introduced at the beginning of this chapter, including those based on lead, nickel, lithium, and sodium–sulfur. The important terms for battery technologies were also introduced. Each technology has unique characteristics for practical applications. Therefore, the selection of the battery was briefly discussed.

Battery technology is still not ideal for widespread use since batteries can be expensive and have limited lifetimes, serious environmental problems, and safety concerns. Lead-acid batteries use sulfuric acid and lead, which are hazardous. Other materials used in batteries, such as nickel, lithium, cadmium, alkalis, and mercury can also contaminate soil and water. Furthermore, fire incidents involving both lithium-ion and NaS batteries raise safety concerns when these technologies are used in high-power-density batteries. Sensing and protection circuits should be carefully designed to guarantee the safe operation of battery power systems.

Battery mismatch and equalization were introduced due to their importance for reliable and long-lifetime operations. A new classification was presented in order to provide

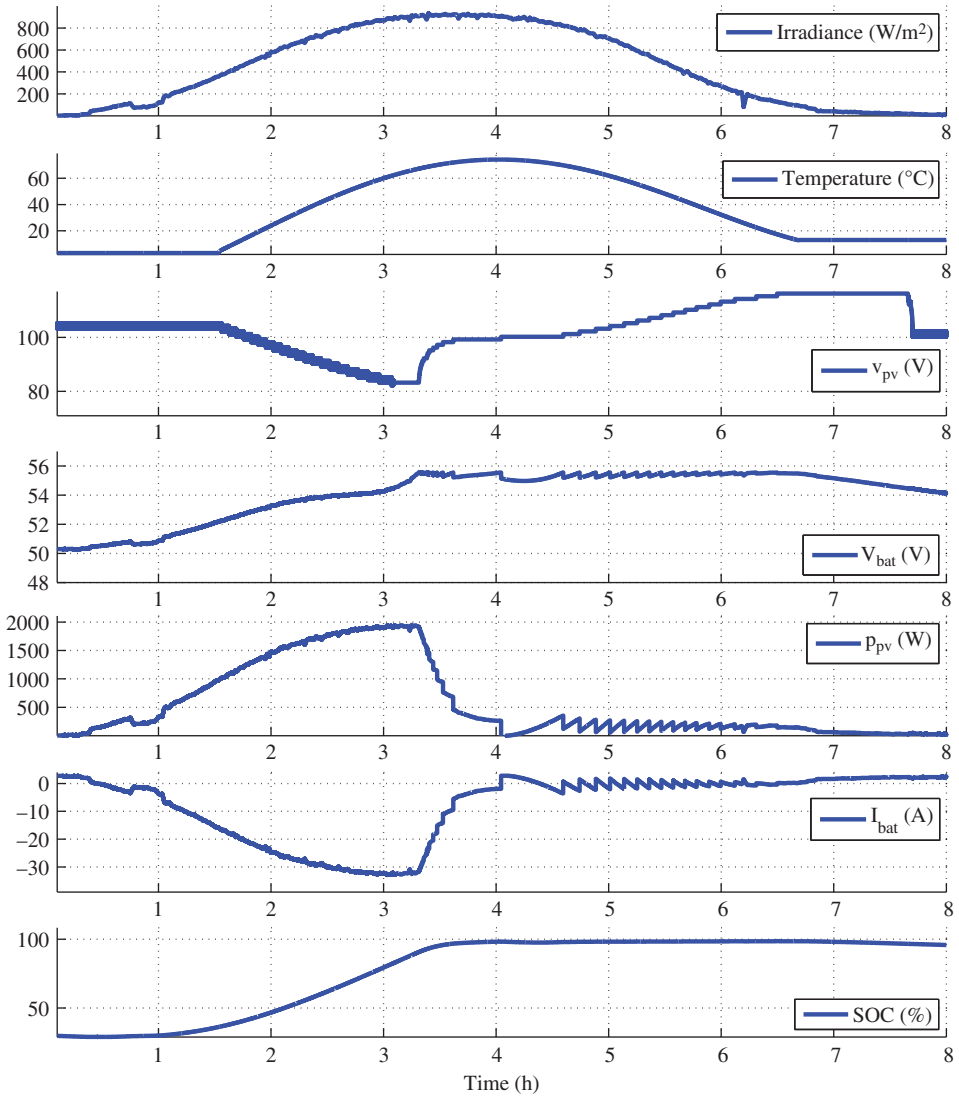

Figure 9.46 Simulation of eight-hour operation of standalone system.

a clear framework for understanding existing methodologies for battery balancing. Even though the case study for equalization was demonstrated mainly at cell level, the same principles can be applied to balance battery modules.

In general, battery modeling is difficult since the parameters are nonlinear and time-variant with many factors, such as the SOC, temperature, age, and frequency. One important development in this chapter concerning battery characteristics and modeling is equivalent circuits at different complication levels. Practical simulation models with the flexibility to represent the battery voltage and the state of charge (SOC) and the option to represent self-discharge were described. Simulations based on Thévenin circuits were built in Simulink and demonstrated for practical implementation. A practical

NiMH battery pack was used to demonstrate the analysis, modeling, simulation, and verification.

The design process of standalone PV systems was discussed. Since most standalone systems contain battery storage, the integration of battery charging and MPPT is described. The algorithm is simple and easy to implement. The design cases for the standalone system with and without battery storage were introduced separately. The direct-coupled system without massive storage represents the simplest standalone PV system, but has significant disadvantages. The typical system is coupled with battery storage and power conditioning to mitigate the intermittent power generation and ensure a steady power supply overnight.

Hybrid system design is not covered, due to the complications for dedicated applications. The knowledge of battery and standalone systems that has been presented in this chapter is useful to design efficient, safe, and reliable hybrid systems.

The simulation of a standalone system is based on one practical design example. The Simulink models for the controller and power interface are developed at different levels for the simulation study: short term, medium term, long term, and very long term. The simulation objective should be always defined clearly to avoid complexity in modeling and inefficiency in simulation. It is always difficult to develop an efficient model, which can simulate not only the long-term changes, but also the transient details of fast dynamics. A simulation of eight hours of system operation shows MPPT, battery voltage regulation, and variation of SOC in response to changes in solar irradiance and cell temperature. The case study neglects the fast dynamics of the switching and PV voltage regulation. The dynamics at the battery link are also ignored for the very-long-term simulation. Without loss of generality, the simulation models are also presented to capture the fast dynamics, including fast switching in the DC/DC converter, but only for short-term simulations due to computational constraints.

Problems

9.1 It is recommended to duplicate the simulation results presented in this chapter. The process is valuable in becoming familiar with the principles of system specification, design, component selection, simulation modeling, system protection, system integration, and verification.

9.2 Use any available simulation tool to construct a battery model based on the presented Thévenin circuits.

9.3 Find a practical battery module or cell to derive the model parameters.

9.4 Verify the simulation model output with the product data.

9.5 Design a PV–battery system for standalone applications.

a) Construct the simulation model to represent the system operation, including the blocks for the PV, battery, MPPT charge controller, and power interface.
b) Simulate the circuit over a short time, to reflect any transient responses that can be caused by sudden changes of load or solar irradiance.